Liquid−Liquid Coexistence Surface for Lysozyme: Role of Salt Type and Salt Concentration

Nathaniel Wentzel* and James D. Gunton

Department of Physics, Lehigh University, Bethlehem, Pennsylvania 18015

Received: August 7, 2006; In Final Form: December 5, 2006

The liquid−liquid phase separation curves for lysozyme in a salt solution are known to depend on salt type and salt concentration. For the case of monovalent cations, the cloud point temperature typically increases with increasing salt concentration, for fixed lysozyme concentration. For the case of divalent cations, however, a maximum in the cloud point temperature is observed that has been interpreted as being due to ion binding to the protein surface and subsequent water structuring. In this paper, we use a simple square well model due to Grigsby et al. (*Biophys. Chem.* **2001**, *91*, 231−243), whose well depth depends on salt type and salt concentration, to determine the phase coexistence surfaces from experimental data. The surfaces are shown as a function of temperature, salt concentration, and protein concentration for two typical salts, NaCl and $MgCl_2$. These surfaces are calculated using the results of a single standard Monte Carlo simulation and a simple scaling argument and are in reasonably good agreement with known experimental results.

1. Introduction

Growing good crystals from solution is a subject of current experimental and theoretical study. Because protein function can be determined by protein structure, it is important to grow high quality crystals in order to determine their structure by X-ray crystallography. The window of optimal crystallization corresponds to small, negative values of the osmotic second virial coefficient, B_2.[1] It is also known that these values of B_2 correspond to protein−protein interactions that are short-ranged with respect to the size of the protein molecule. This typically corresponds to salt concentrations sufficiently large to screen the Coulomb repulsive interaction, so that the Debye screening length is small. The net short-range attractive interaction yields a metastable liquid−liquid phase separation that is thought to be responsible for the optimal crystal nucleation.[2,3] In this paper, we consider the Hofmeister effect on the liquid−liquid phase separation.

The Hofmeister effect, first studied in the 1800s,[4,5] is the name given to the phenomenon where different salt types induce different effects on protein precipitation and phases. In particular, there are extensive experimental studies of the Hofmeister effect for lysozyme. These include the effects of salt concentration and salt type on the solubility (liquidus) curve[6−9] and on the metastable liquid−liquid phase separation curve.[6−14] The Hofmeister effect has long been a mystery. In particular, the classic DLVO theory[15,16] that accounts for the effects of salt on colloid or protein precipitation does not depend on salt type. Because DLVO lacks salt-specific input, it cannot explain the Hofmeister effect. Many possible explanations have been proposed including salt-specific ion-dispersion forces between the salt ions and protein molecules,[17] hydration forces, water structure, and dissolved gas.[18] Despite recent progress involving the ion-dispersion forces,[17] no detailed theory exists for the effects of salt type on the phase diagrams of globular proteins.

In this paper, we focus on the Hofmeister effect in lysozyme, specifically in the metastable liquid−liquid phase separation that has been experimentally observed. Two quite different behaviors of the cloud point temperature with salt concentration have been observed.[10] For a fixed protein concentration, adding salt with a monovalent cation, such as NaCl, causes the cloud point temperature to increase with salt concentration. However, for salts with divalent cations, such as $MgCl_2$, the cloud point temperature passes through a maximum and then decreases. In ref 10, this effect is interpreted as being due to the highly kosmotropic nature of the divalent cation. In the presence of a kosmotropic ion, water binds more strongly than without the ion, yielding more structured water with a lower entropy.

A simple model that has been used to describe protein interactions is the square well model (defined in more detail in section 2). This phenomenological model for protein−protein interaction is an approximate description of the short-ranged attractive forces (such as the van der Waals interaction, ion-dispersion forces, and hydration forces), obtained by varying the depth and range of the attractive well. Although this model is a crude approximation for the spatial description of the forces between proteins, it has been shown to provide a reasonably accurate description of the liquid−liquid phase diagram for globular proteins in solution.[19,20] For a fixed salt type, this model yields a semiquantitative description of the phase diagrams of these systems.

In refs 10 and 14, salt-specific effects on the protein−protein interactions are modeled by assuming a square well depth that depends on both salt concentration and salt type. The range of attraction of the well is kept constant, presumably for simplicity. The random phase approximation (RPA) is used to obtain expressions for the pressure, P, and chemical potential, μ, for the protein-rich and protein-poor fluid phases. For a fixed lysozyme concentration, fits to the experimental data for the cloud point temperature, T, as a function of salt concentration for a particular salt are used as inputs for the cloud point temperature in the expressions for P and μ. P and μ also include a perturbation energy that takes into account interactions beyond

* Corresponding author. E-mail: njw4@lehigh.edu. Fax: (610) 758-5730.

10.1021/jp065062b CCC: $37.00
Published on Web 01/23/2007

the hard sphere interaction. These can be expressed using the square well as the potential of mean force between the protein molecules. The square well depths as a function of salt concentration, $\epsilon(I)$, are then found from the conditions for two-phase coexistence, which require that P and μ are equal, for each salt concentration, I. This phenomenological model provides a useful way in which to obtain an estimate of the interactions (dependent on salt type and salt concentration) from experimental data.

In this paper, we use the square well model to extend the approach of these authors[10] and obtain an approximate form for the liquid−liquid coexistence surface representing the lysozyme liquid−liquid phase separation temperature as a function of the concentrations of both the protein and salt. Our basic observation is that if one uses such a square well model with a fixed range of interaction but variable well depth, then a simple scaling argument yields the coexistence surface from a single liquid−liquid coexistence curve for a given salt of fixed concentration. Because RPA is a mean-field approach which is not accurate for short-range forces such as our model,[12] we determine the coexistence curve by using results from a Monte Carlo simulation of the square well model.[21] We determine the well depth in this model from the experimental cloud point data. At a single protein concentration, the dependence of the cloud point curve on salt concentration immediately gives the square well depth as a function of salt concentration.

The outline of the paper is as follows. In section 2, we explain how we use measured temperatures as a function of salt concentration, $T(I)$, to find $\epsilon(I)$ and to generate a liquid−liquid coexistence surface using Monte Carlo results from an earlier simulation.[21] In section 3, we apply this method to two cases that exhibit qualitatively different coexistence surfaces, NaCl and $MgCl_2$. In section 4, we present a brief conclusion.

2. Model

The isotropic square well is defined as

$$V(r) = \begin{cases} \infty, & r < \sigma \\ -\epsilon, & \sigma \le r < \lambda\sigma \\ 0, & r \ge \lambda\sigma \end{cases} \tag{1}$$

where σ is the hard core, taken to be the protein diameter, λ is a constant describing the width of the well, and ϵ is the well depth.

Because the only dependence on the well depth, ϵ, and temperature in the square well model is through the ratio ϵ/kT in the Boltzmann factor, the free energy depends on temperature only through this ratio. Consequently, the temperatures used in square well simulations are $\tilde{T} \equiv kT/\epsilon$. Our approach is to directly convert the simulated coexistence curve from scaled temperatures to real temperatures using the measured dependence of the cloud points on salt concentration, finding $\epsilon(I)$ by unscaling the temperature results from the dimensionless temperature units in the simulation to the temperatures found in experiments.

The measured cloud point temperatures in ref 10 were found for a constant protein concentration, $\rho = \rho_0$, used as a reference value for our scaling. For our calculations, we express ρ_0 as the volume fraction of protein. Let $T_0(I) \equiv T(I,\rho_0)$ represent the cloud point temperature as a function of salt concentration, I, for a given type of salt at fixed volume fraction ρ_0. Also, let $\tilde{T}_0 \equiv kT(\rho_0)/\epsilon$ be the scaled temperature in the simulations for volume fraction ρ_0, and let $\tilde{T}(\rho)$ be the coexistence curve obtained from simulation. The coexistence surface is then generated by

$$T(I,\rho) = \frac{\tilde{T}(\rho)}{\tilde{T}_0} T_0(I) \tag{2}$$

We have assumed that the cloud point temperature, for a given salt, has the same dependence on I for all volume fractions of the protein. In particular, this is chosen to be the dependence on I found for the reference volume fraction ρ_0. Equation 2 was found by equating the ratio of T to T_0 for both ρ_0 and all ρ.

From our definition of $\tilde{T}$, we can calculate values for ϵ as a function of salt concentration. For the reference volume fraction ρ_0, we have

$$\frac{\epsilon(I)}{k} = \frac{T_0(I)}{\tilde{T}_0} \tag{3}$$

This ϵ value could be used to perform simulations for each I in order to generate the phase coexistence surface. A set of such simulations would produce the same results as a single simulation and using eq 2.

One advantage of using the isotropic square well model for the protein pair potential is that the osmotic second virial coefficients can be found exactly. Knowing the depth, ϵ, for a square well allows us to calculate second virial coefficients exactly. The second virial coefficient, defined as the coefficient of the leading term in the expansion of the osmotic equation of state, is given in terms of an integral of the pair potential[22]

$$B_2 = 2\pi \int_0^\infty r^2 (1 - e^{-V(r)/kT})\, dr \tag{4}$$

where $V(r)$ is the protein pair potential. Using the square well model for $V(r)$, B_2 follows exactly from eq 4 as

$$B_2 = \frac{2\pi\sigma^3}{3}[\lambda^3 - e^{\epsilon/kT}(\lambda^3 - 1)] \tag{5}$$

This gives us B_2 as a function of salt concentration through its dependence on the concentration dependent well depth. Note that in our model, as in ref 10, λ is a fixed value that does not depend on I. This is somewhat unrealistic, as one would expect the range as well as the well depth to depend on I, but the choice of a fixed range simplifies the calculation.

3. Results

To generate liquid−liquid phase coexistence surfaces, we use eq 2, which requires our expressions for $T_0(I)$, $\tilde{T}(\rho)$, and $\tilde{T}_0$. To demonstrate the model, we use the data from ref 10. We fit the cloud point measurements as a function of salt concentration for pH = 7.0 and pH = 4.0 solutions, but we note that the model could be applied to cloud point temperatures versus salt concentration for any pH. Also, although we could use any of the salts studied in ref 10 or 14, we here consider only two salts, NaCl and $MgCl_2$, that illustrate two qualitatively different effects observed in the experiments. The functional forms we use for the fits are arbitrary but provide a convenient way to represent that data. For pH = 7.0, the best fit for NaCl is

$$T_0(I) = 22.3 \ln(I) + 303 \tag{6}$$

and for $MgCl_2$ is

$$T_0(I) = 260 + 43.2I - 23.4I^2 \tag{7}$$

while, for pH = 4.0, the best fit for NaCl is

$$T_0(I) = 29.4 \ln(I) + 300 \tag{8}$$

and for $MgCl_2$ is

$$T_0(I) = 266 + 40.7I - 18.4I^2 \tag{9}$$

The data used for these fits were taken for lysozyme with a concentration of 87 mg·mL^{-1} which corresponds to the volume fraction $\rho_0 = 0.0716$ in simulation. Although we use the same functional form as ref 10 for NaCl (eqs 6 and 8), we use a different form for $MgCl_2$ (eqs 7 and 9), as it gives a somewhat better fit to the data. The fit in eq 6 also compares well with the fit to NaCl cloud points found in ref 8.

Our scaled coexistence curve, $\tilde{T}(\rho)$, is taken from square well simulations with $\lambda = 1.15$. Figure 1 shows the low density portion of the liquid−liquid coexistence curve obtained from simulation (see ref 21) along with measurements of liquid−liquid coexistence for lysozyme (see refs 9 and 11). The lysozyme measurements were made for pH = 4.5 solutions with various NaCl concentrations. We have scaled the experimental measurements using our results for $T_0(I)$ from eq 8. The simulation results show semiquantitative agreement with the experiment, sufficient for the purpose of this paper. In ref 10, Grigsby et al. chose $\lambda = 1.20$, but we note that in ref 21 the liquid−liquid coexistence curves from simulations of square wells with $\lambda = 1.15$ and $\lambda = 1.25$ have similar shapes. It follows then that the liquid−liquid curves for $\lambda = 1.20$ and $\lambda = 1.15$ should also have similar shapes.

In the simulation results for $\lambda = 1.15$, we find that the reference volume fraction $\rho_0 = 0.0716$ corresponds to a scaled coexistence temperature of $\tilde{T}_0 = 0.535$. We generate the phase coexistence surface for NaCl using eqs 2 and 6 and for $MgCl_2$ using eqs 2 and 7 and the values for ρ_0 and $\tilde{T}_0$. The results for pH = 7.0 are displayed in Figures 2 and 3. These figures qualitatively resemble the surfaces for a pH = 4.0 solution (not shown). Note the qualitatively different behavior between the two salts, which corresponds to the qualitatively different behavior of their cloud point temperatures as a function of salt concentration. For NaCl, the coexistence temperature for each lysozyme concentration increases with increasing salt concentration, while, for $MgCl_2$, the coexistence temperature for each lysozyme concentration reaches a maximum as the salt concentration increases.

We find $\epsilon(I)$ using eq 3 and the appropriate equation for $T_0(I)$. For NaCl and $MgCl_2$ in a pH = 7.0 solution, we find, respectively,

$$\frac{\epsilon(I)}{kT_{25}} = 0.140 \ln(I) + 1.90 \tag{10}$$

$$\frac{\epsilon(I)}{kT_{25}} = 1.63 + 0.271I - 0.147I^2 \tag{11}$$

For NaCl and $MgCl_2$ in a pH = 4.0 solution we find, respectively,

$$\frac{\epsilon(I)}{kT_{25}} = 0.185 \ln(I) + 1.88 \tag{12}$$

$$\frac{\epsilon(I)}{kT_{25}} = 1.67 + 0.255I - 0.115I^2 \tag{13}$$

where we use $T_{25} = 298$ K as a reference temperature for the model, following ref 10.

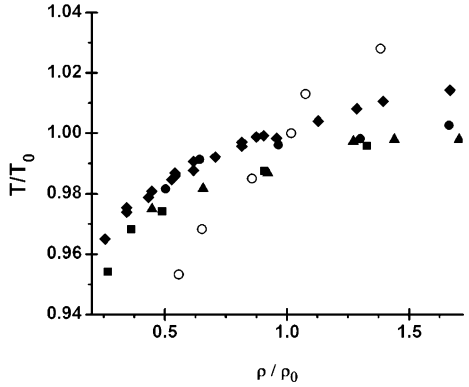

Figure 1. Comparison of simulated liquid−liquid separation for $\lambda = 1.15$ from ref 21 (open circles) with measured points for NaCl at four concentrations, 3% (filled circles), 5% (triangles), and 7% (squares) from ref 9 and 4% (diamonds) from ref 11.

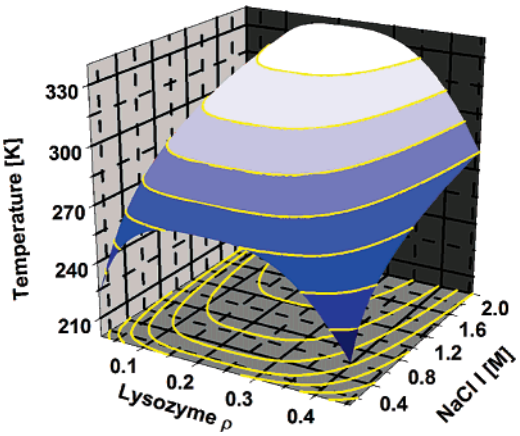

Figure 2. Liquid−liquid coexistence surface for lysozyme in NaCl from the model.

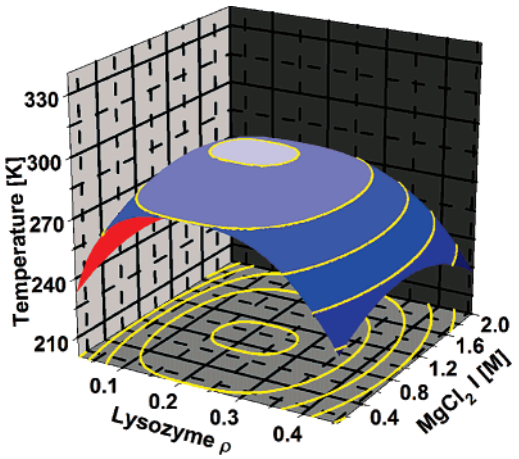

Figure 3. Liquid−liquid coexistence surface for lysozyme in $MgCl_2$ from the model.

The expressions for $\epsilon(I)$ from eqs 10−13 can be used with eq 5 to find second virial coefficients, B_2, as a function of salt concentration. In Figure 4, we show the second virial coefficients, normalized by $B_2^{HS} = 2\pi\sigma^3/3$, for a pH = 4.0 solution with temperature T_{25}. The results for pH = 7.0 are similar. Note that, for NaCl, the second virial coefficient is decreasing as a function of salt concentration, while, for $MgCl_2$, the second virial coefficient first decreases and then increases with salt concentration. The line from the model for NaCl at pH = 4.0 follows closely with experimental data for pH ≈ 4.5 compiled from various sources in ref 23.

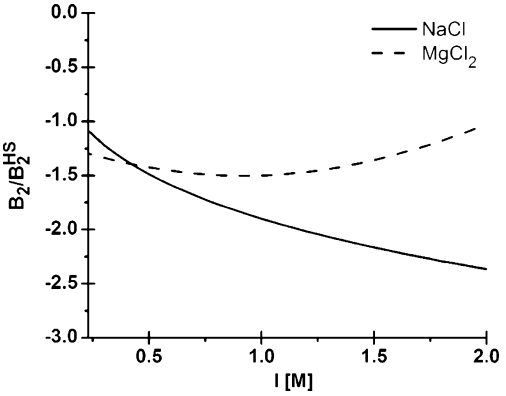

Figure 4. B_2/B_2^{HS} for NaCl and $MgCl_2$ from the model.

It is important to note that we use a model with a short-range attraction, a square well with $\lambda = 1.15$, in a regime where the net lysozyme interaction is attractive. In experiments at low salt concentrations, however, the proteins will undergo a net repulsion and the second virial coefficient, B_2, will be positive. Such experiments are not, however, performed in a regime where the metastable liquid−liquid curve exists. Because our model uses a (simulated) metastable liquid−liquid curve, it cannot be applied to low salt concentrations, *I*, that correspond to a repulsive net lysozyme interaction and give a positive value for B_2.

4. Conclusion

We have developed a method to generate phase coexistence surfaces for lysozyme in solution with various salts. The method depends on knowing the liquid−liquid coexistence temperature of a solution with a fixed single protein concentration, as a function of salt concentration for a given salt. We use a square well interaction and use the simple scaling property of a square well model to generate the surfaces from a Monte Carlo simulation of a square well model with a single well depth. We have studied the Hofmeister effect for two salts exhibiting qualitatively different behaviors of liquid−liquid phase separation as a function of salt concentration. We also give second virial coefficients as a function of salt concentration for both salt types.

We conclude by noting some limitations of our model. First, because the square well model provides only a semiquantitative description of the lysozyme liquid−liquid coexistence curve, we expect that these coexistence surfaces provide only a semiquantitative description of the real lysozyme behavior. However, because we use a square well, this method can be used to model the Hofmeister effect in phase diagrams of other proteins such as γ-crystallins (see, for example, refs and 19 and 20).

Second, our model cannot be used to predict accurately the behavior of the solubility curve using data from the cloud points. This is due to the fact that the dependence of the solubility curve on salt concentration is not the same as the dependence of cloud points on salt concentration (see ref 8). Although we cannot use measured liquid−liquid phase separation data to model a liquid−solid coexistence, it may be possible to apply our model to the solubility curve using measured solubility temperatures as a function of salt concentration.

Another limitation of our model is that we use the same dependence on salt concentration for all protein concentrations. The critical temperatures in ref 9, which are measured at lysozyme concentrations different from the fixed lysozyme concentration used in ref 10, do not show the same dependence on salt concentration as the cloud point temperatures in ref 10. Our model also depends on a fixed range of interaction, λ, between the protein molecules for all protein concentrations. Changing λ as a function of protein concentration could overcome the difference in dependence on *I* for different protein concentrations, but this would clearly obviate the simplicity of our approach. As it is presented, the model provides a simple approach for using experimental data to obtain a semiquantitative prediction for the phase diagram and second virial coefficients of globular proteins as a function of salt concentration for a given salt type.

Acknowledgment. This work was supported by the G Harold and Leila Y. Mathers Foundation and by the National Science Foundation grant DMR-0302598.

References and Notes

(1) George, A.; Wilson, W. *Acta Cryst.* **1994**, *D50*, 361−365.
(2) Rosenbaum, D.; Zamora, P. C. ; Zukoski, C. F. *Phys. Rev. Lett.* **1996**, *76*, 150−153.
(3) Gunton, J. D.; Shiryayev, A.; Pagan, D. L. *Protein Condensation: Kinetic Pathways to Crystallization and Disease*; Cambridge University Press: Cambridge, England, 2007.
(4) Hofmeister, F. *Arch. Exp. Pathol. Pharmakol.* **1888**, *24*, 247−260.
(5) Leweth, S. *Arch. Exp. Pathol. Pharmakol.* **1888**, *24*, 1−16.
(6) Ishimoto, C.; Tanaka, T. *Phys. Rev. Lett.* **1977**, *39*, 474−477.
(7) Taratura, V. G.; Holschbach, A.; Thurston, G. M.; Blankenstein, D.; Benedek, G. B. *J. Phys. Chem.* **1990**, *94*, 2140−2144.
(8) Broide, M. L.; Tominc, T. M.; Saxowsky, M. D. *Phys. Rev. E* **1996**, *53*, 6325−6335.
(9) Muschol, M.; Rosenberger, F. *J. Chem. Phys.* **1997**, *107*, 1953−1962.
(10) Grigsby, J. J.; Blanch, H. W.; Prausnitz, J. M. *Biophys. Chem.* **2001**, *91*, 231−243.
(11) Petsev, D. N.; Wu, X.; Galkin, O.; Vekilov, P. G. *J. Phys. Chem. B* **2003**, *107*, 3921−3926.
(12) Manno, M.; Xiao, C.; Bulone, D.; Martorana, V.; San, Biagio, P. L. *Phys. Rev. E* **2003**, *68*, 011904.
(13) Lu, J.; Carpenter, K.; Li, R.; Wang, X.; Ching, C. *Biophys. Chem.* **2004**, *109*, 105−112.
(14) Park, E. J.; Bae, Y. C. *Biophys. Chem.* **2004**, *109*, 169−188.
(15) Derjaguin, B. V.; Landau, L. *Acta Physicochim. URSS* **1941**, *14*, 633−662.
(16) Verwey, E. J. W.; Overbeek, J. T. G. *Theory of stability of Lyophobic Colloids*; Elsevier: Amsterdam, The Netherlands, 1948.
(17) Kunz, W.; Henle, J.; Ninham, B. W. *Curr. Opin. Colloid Interface Sci.* **2004**, *9*, 1−18.
(18) Boström, M.; Williams, D. R. M.; Ninham, B. W. *Biophys. J.* **2003**, *85*, 686−694.
(19) Asherie, N.; Lomakin, A.; Benedek, G. B. *Phys. Rev. Lett.* **1996**, *77*, 4832−4835.
(20) Asherie, N. *Methods* **2004**, *34*, 266−272.
(21) Pagan, D. L.; Gunton, J. D. *J. Chem. Phys.* **2005**, *122*, 184515.
(22) Hill, T. L. *An introduction of Statistical Thermodynamics*; Dover: New York, 1986.
(23) Prinsen, P.; Odijk, T. *J. Chem Phys.* **2004**, *121*, 6525−6537.